Eur. Phys. J. A **6**, 141–147 (1999)

THE EUROPEAN PHYSICAL JOURNAL A

Spectroscopy of ^{200}Hg after incomplete fusion reaction

A. Görgen[1], H. Hübel[1], D. Ward[2], S. Chmel[1], R.M. Clark[2], M. Cromaz[2], R.M. Diamond[2], P. Fallon[2], K. Hauschild[3,a], G.J. Lane[2], I.Y. Lee[2], A.O. Macchiavelli[2], K. Vetter[2]

[1] Institut für Strahlen- und Kernphysik, Universität Bonn, Nussallee 14-16, 53115 Bonn, Germany
[2] Lawrence Berkeley National Laboratory, Berkeley, CA 94720, USA
[3] Lawrence Livermore National Laboratory, Livermore, CA 94550, USA

Received: 8 June 1999
Communicated by B. Herskind

Abstract. High–spin states in ^{200}Hg have been investigated by in–beam γ–ray spectroscopy following the reaction ^{198}Pt(^{9}Be,α3n). The α–emission channel leading to ^{200}Hg is strongly enhanced which may be explained by an incomplete fusion reaction with pre–equilibrium emission of the α particle. The level scheme is extended to higher spins and new band crossings are observed. The band structures are compared to the lighter Hg isotopes with even mass number.

PACS. 21.10.-k Properties of nuclei; nuclear energy levels – 23.20.Lv Gamma transitions and level energies – 23.20.En Angular distribution and correlation measurements – 25.70.Jj Fusion and fusion-fission reactions – 27.80.+w $190 \leq A \leq 219$

1 Introduction

In the weakly oblate deformed Hg isotopes with mass numbers between A = 190 and 198 the level schemes are dominated by collective rotational bands built on the ground state and on quasineutron excitations. The properties of these band structures are well described within the framework of the cranked shell model (CSM). The Hg isotopes were the first cases in which the CSM was successfully applied to weakly oblate nuclei [1,2]. Alignment frequencies and aligned angular momenta of $i_{13/2}$ quasineutrons were well reproduced by the model. In the case of ^{200}Hg, the $\nu i_{13/2}$ subshell is filled and a large gap appears in the Nilsson energy–level diagram. Therefore, one expects the band structures based on excitations in the $\nu i_{13/2}$ subshell to have higher excitation energy. Experimental information on this energy is important for a comparison with different calculations and for the prediction of the location of states involving excited $i_{13/2}$ neutrons.

We have investigated ^{200}Hg by in–beam γ–ray spectroscopic techniques after an incomplete fusion reaction. The only combination of stable projectile and target to populate the nucleus ^{200}Hg in a conventional heavy ion induced fusion reaction followed by neutron evaporation is ^{198}Pt(α,2n)^{200}Hg. The angular momentum input into the compound system is limited in this reaction because of the small mass of the projectile and since the optimum beam energy is close to the Coulomb barrier. In an experiment using the (α,2n) reaction at beam energies of 26 to 28 MeV states up to spin $I = 14\hbar$ have been identified [3]. This is the maximum spin one can expect to observe in this reaction even with the highly efficient γ–ray spectrometers which are available nowadays.

An alternative method to populate a nucleus close to stability in a fusion evaporation reaction with a higher angular momentum input would be the use of a neutron–rich radioactive ion beam. However, such beams are currently not available with sufficient intensities. In the case of ^{200}Hg a neutron rich beam is already available in a sense, since one can use the break–up of a ^{9}Be projectile in an incomplete fusion reaction. For the ^{198}Pt + ^{9}Be reaction used in our work this corresponds to the reaction ^{198}Pt(^{5}He,3n)^{200}Hg. Due to the peripheral character of incomplete fusion reactions [4] significantly more angular momentum is transferred to the compound system compared to the (α,2n) complete fusion reaction. Indeed, in this work states are observed up to spin $21\hbar$.

2 Experimental methods and data analysis

The beam of ^{9}Be at 60 MeV was provided by the 88–Inch Cyclotron of the Lawrence Berkeley National Laboratory. The target consisted of an 18mg/cm^2 thick foil of ^{198}Pt. Gamma–ray spectroscopy was performed with the 8π spectrometer which comprises 20 Ge detectors with BGO Compton–suppression shields, and an inner spherical shell of 71 BGO scintillation detectors. Events were

[a] *Present address:* DAPNIA/SPhN, CEA Saclay, F-91191 Gif-sur-Yvette Cedex, France
Correspondence to: goergen@iskp.uni-bonn.de

Table 1. Experimental relative yields for the reaction ^{9}Be + ^{198}Pt at $E_{beam} = 60$ MeV and simulation using the code PACE. The yields are normalized to the strongest channel leading to ^{202}Pb

	^{201}Pb	^{202}Pb	^{203}Pb	^{199}Hg	^{200}Hg
experiment	28(5)	100	17(4)	8(2.5)	39(7)
PACE	26	100	11	0.11	0.04

written to tape when two or more Ge detectors and three or more BGO detectors of the inner ball gave coincident signals. During the 15 shifts of beamtime 115×10^6 two–fold, 6.5×10^6 three–fold and 2.7×10^5 four–fold events were written to tape. In the off–line analysis the three– and four–fold events were split up into doubles, resulting in a total of 136×10^6 events with fold two.

The scintillation detectors of the inner ball were used to select events with a high multiplicity and to distinguish between different reaction channels. The yields of the channels populated in the reaction are given in Table 1. For comparison the results of a calculation performed with the code PACE [5] are also given which takes into account only fusion evaporation but no pre–equilibrium emission of projectile fragments. In the PACE calculations the energy loss of the beam in the thick target was taken into account. It is obvious that the strong population of the Hg isotopes cannot be explained only by particle evaporation of the equilibrated compound system. It has been shown in previous studies [6], using γ–α coincidence techniques, that in ^{9}Be induced reactions the emission of α particles is strongly enhanced and peaked into forward directions. This can be understood by the break–up of the ^{9}Be projectile with pre–equilibrium emission of the α particle and fusion of the ^{5}He fragment. The measurement of excitation functions, momentum and angular momentum transfer in incomplete fusion reactions has been the subject of many investigations, e.g. [4,6–9] and several models have been proposed [4,10,11]. The experimental relative yields and the angular momentum transfer observed in this work agree well with the assumption of incomplete fusion and thus we conclude that this process plays a major rule in the population of ^{200}Hg.

The coincident γ–rays measured with the Ge–detector array were sorted into a variety of E_γ–E_γ matrices with different conditions on the multiplicity K and sum energy H in the inner ball of BGO scintillation detectors. Examples of the γ–ray coincidence spectra are shown in Fig. 1. A multiplicity of seven γ rays in the inner ball was required.

Two different methods to analyze γ–γ directional correlations (DCO) were used to obtain information on the multipolarities of the γ–ray transitions. The first method, which we refer to as method A, is the one that is normally used to obtain DCO ratios [12]. The Ge detectors are mounted in four rings located at angles of $\pm 37^o$ and $\pm 79^o$ with respect to the beam axis. The DCO ratio of method A is defined as

$$R^{(A)}_{DCO}(E, E_G) = \frac{1}{N} \frac{I_{37,79}(E, E_G)}{I_{79,37}(E, E_G)}, \qquad (1)$$

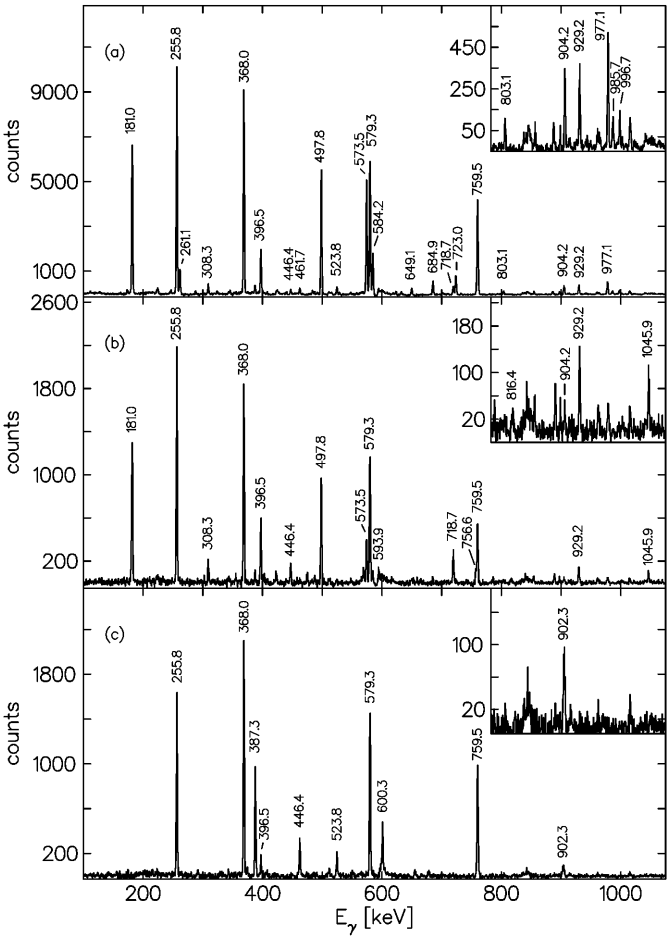

Fig. 1. Gamma–ray coincidence spectra showing the AB band (a), the AE band (b) and the AF band (c). Spectrum (a) is the sum of spectra gated on the 396.5, 584.2, 723.0 and 997.1 keV transitions. Spectrum (b) was created by adding the spectra gated on all in–band transitions above the 11^- state. For spectrum (c) the two spectra with gates on the 172.7 and the 342.3 keV transitions were added. Peaks which are not labeled are contaminations from the Pb nuclei produced in complete fusion reactions. The insets show the high–energy part of the spectra with an enlarged scale

where $I_{\theta_1,\theta_2}(E, E_G)$ is the intensity of a peak with energy E observed at angles $\pm\theta_1$ when gated on a transition with energy E_G detected at angles $\pm\theta_2$. This ratio is normalized by a factor N to known stretched quadrupole transitions observed in the same spectrum. The normalization is needed because gates were set on transitions regardless of their multipole character.

In the second method [13], method B, coincidences of pairs of γ–rays detected at the same angles $\pm\theta$ were analyzed. Therefore two matrices corresponding to $\pm 37^o$ and $\pm 79^o$ correlations were sorted. The second DCO ratio is then defined as

$$R^{(B)}_{DCO}(E, E_G) = \frac{I_{37,37}(E, E_G)}{I_{79,79}(E, E_G)} \qquad (2)$$

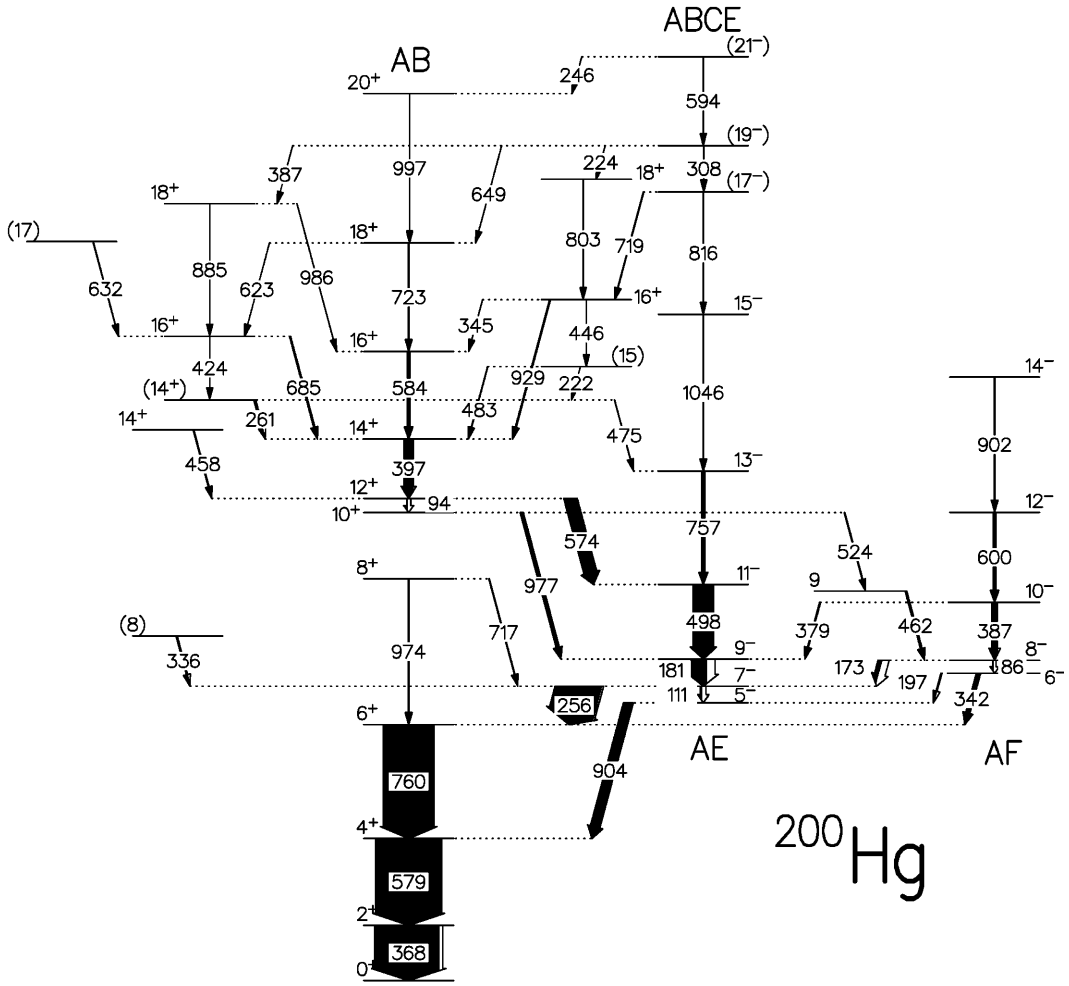

Fig. 2. Level scheme of ^{200}Hg obtained in the present work. The width of the arrows is proportional to the intensity of the transitions, while the white part of the arrows is the correction due to internal conversion. The strongly populated states up to I = 14 are in agreement with previous work [3]

In this case only stretched E2 transitions were used as gates, therefore no normalization is needed.

All spectra were corrected for detection efficiencies and background was subtracted. Theoretical DCO ratios were calculated for both methods under the following assumptions: The nucleus is populated at spin $J = 17$ with a spin alignment described by a Gaussian distribution of m substates with a standard deviation σ. The dimensionless factor σ/J is regarded as a constant for a given reaction and can be fitted for cascades of stretched E2 transitions, resulting in $\sigma/J = 0.35 \pm 0.04$ in our case. The initial state is assumed to decay by unobserved stretched transitions to the state of interest. DCO ratios were calculated for various γ–γ correlations as a function of σ/J, J and M1/E2 mixing ratio δ. In Table 2 results are given for a few special cases.

Both ratios distinguish clearly between stretched dipole and quadrupole transitions whereas it is impossible to distinguish between stretched quadrupole and $\Delta I = 0$ transitions. Nevertheless, the use of both methods has been advantageous to reach a decision in cases of very weak transitions.

Table 2. Calculated DCO ratios for three $\gamma - \gamma$ cascades $I_i \rightarrow I \rightarrow I_f$ under the assumptions described in the text. Values are given for $\delta = 0$ and $\sigma/J = 0.35$

	$17 \rightarrow 17 \rightarrow 15$	$17 \rightarrow 16 \rightarrow 14$	$17 \rightarrow 15 \rightarrow 13$
$R^{(A)}_{DCO}$	1.05	0.66	1.00
$R^{(B)}_{DCO}$	1.74	1.10	1.66

Gamma–ray transition energies, relative γ–ray and total transition intensities, DCO ratios and assignments are given in Table 3.

3 Level scheme

In the present work 53 transitions connecting 35 levels in ^{200}Hg were identified to establish the level scheme shown in Fig. 2. The placement of the transitions is based on

Table 3. Energies, intensities, DCO ratios and assignments of γ–ray transitions in ^{200}Hg. Theoretical values for the two different DCO ratios A and B are given in Table 2 for stretched and non–stretched dipole and quadrupole transitions

Energy	rel. Intensity		R_{DCO}		Multip.	Energy Level	Assignment		
E_γ(keV)	I_γ	I_{tot}	A	B		E_i(keV)	I_i^π	→	I_f^π
86.4			a		E2	2135.4	8^-	→	6^-
94.2	9(4)	73	b	b	E2	3214.9	12^+	→	10^+
110.7	17(1.4)	90	0.88(19)	b	E2	1962.6	7^-	→	5^-
172.7	55(4)	171	0.75(9)	1.09(15)	M1	2135.4	8^-	→	7^-
181.0	230(9)	374	1.03(10)	1.61(16)	E2	2143.6	9^-	→	7^-
197.4	7.1(1.1)	17.3	0.77(12)	0.72(26)	M1	2049.0	6^-	→	5^-
221.7	1.0(0.4)	c	0.69(28)	b	c	4094.3	(15)	→	(14)
224.0	2.6(0.8)	(2.7)	0.62(10)	0.94(21)	(E1)	5568.3	(19^-)	→	18^+
246.4	0.6(0.3)	(0.6)	0.48(32)	b	(E1)	6162.2	(21^-)	→	20^+
255.8	700(24)	730	0.64(6)	0.91(12)	E1	1962.6	7^-	→	6^+
261.1	18.5(2.2)	(29)	1.03(10)	1.43(13)	(M1)	3872.7	(14^+)	→	14^+
308.3	4.0(1.0)	4.4	1.00(14)	1.85(24)	E2	5568.3	(19^-)	→	(17^-)
336.1	15.0(2.4)	c	0.63(7)	1.01(12)	c	2298.6	(8)	→	7^-
342.3	63(5)	64	1.04(11)	1.33(16)	E1	2049.0	6^-	→	6^+
345.1	1.8(0.5)	2.4	0.71(34)	b	M1	4540.9	16^+	→	16^+
368.0	1000	1066	0.99(8)	1.50(12)	E2	368.0	2^+	→	0^+
378.9	14.2(1.3)	17.6	0.96(27)	0.97(25)	M1	2522.7	10^-	→	9^-
386.8	0.4(0.2)	(0.4)	0.52(20)	b	(E1)	5568.3	(19^-)	→	18^+
387.3	84(8)	85	0.96(11)	1.76(18)	E2	2522.7	10^-	→	8^-
396.5	135(8)	142	0.97(11)	1.70(16)	E2	3611.4	14^+	→	12^+
423.7	2.9(0.6)	c	0.84(14)	b	c	4296.4	16^+	→	(14)
446.4	0.8(0.4)	c	0.92(19)	b	c	4540.9	16^+	→	(15)
457.8	11.0(1.7)	11.4	1.06(22)	1.88(31)	E2	3672.7	14^+	→	12^+
461.7	24(2)	c	0.65(10)	1.36(18)	c	2597.1	(9)	→	8^-
474.8	3.4(0.7)	(3.4)	0.82(21)	b	(E1)	3872.8	(14^+)	→	13^-
482.9	5.5(0.8)	c	0.72(14)	1.43(35)	c	4094.3	(15)	→	14^+
497.8	305(12)	314	1.06(9)	1.48(15)	E2	2641.4	11^-	→	9^-
523.8	11.3(1.0)	c	0.61(8)	b	c	3120.7	10^+	→	(9)
573.5	202(10)	203	0.61(6)	1.03(12)	E1	3214.9	12^+	→	11^-
579.3	1005(30)	1026	1.06(11)	1.62(14)	E2	947.3	4^+	→	2^+
584.2	37(2.8)	38	1.08(9)	1.69(14)	E2	4195.6	16^+	→	14^+
593.9	1.2(0.5)	1.2	0.86(17)	b	E2	6162.2	(21^-)	→	(19^-)
600.3	39(3)	39	1.05(10)	1.70(18)	E2	3123.0	12^-	→	10^-
622.6	3.0(0.6)	3.1	b	b	E2	4918.9	18^+	→	16^+
631.6	5.0(0.9)	c	0.60(12)	b	c	4928.0	(17)	→	16^+
649.1	0.8(0.3)	(0.8)	0.52(9)	b	(E1)	5568.3	(19−)	→	18^+
684.9	18.6(2.8)	18.9	0.91(14)	1.49(19)	E2	4296.4	16^+	→	14^+
716.8	3.1(1.0)	3.1	b	b	E1	2680.4	8^+	→	7^-
718.7	8.8(1.5)	(8.8)	0.67(9)	0.86(14)	(E1)	5259.8	(17^-)	→	16^+
723.0	11.9(1.0)	12.0	1.06(13)	1.55(22)	E2	4918.6	18^+	→	16^+
756.6	44(6)	45	1.05(15)	1.78(26)	E2	3398.0	13^-	→	11^-
759.5	785(24)	799	0.99(8)	1.63(15)	E2	1706.8	6^+	→	4^+
803.1	4.9(0.9)	5.0	1.10(23)	1.38(34)	E2	5344.1	18^+	→	16^+
816.4	1.1(0.5)	(1.1)	b	b	(E2)	5259.8	(17^-)	→	15^-
885.0	2.7(0.6)	2.7	1.18(19)	1.47(30)	E2	5181.3	18^+	→	16^+
902.3	9.4(1.6)	9.5	0.83(15)	1.62(31)	E2	4025.3	14^-	→	12^-
904.2	150(6)	151	0.68(6)	0.97(10)	E1	1851.5	5^-	→	4^+
929.2	13.7(1.9)	13.8	0.93(14)	1.53(24)	E2	4540.9	16^+	→	14^+
973.6	16.9(2.4)	17.0	1.06(13)	1.46(21)	E2	2680.4	8^+	→	6^+
977.1	49(4)	49	0.64(9)	0.95(11)	E1	3120.7	10^+	→	9^-
985.7	2.5(0.5)	2.5	0.73(18)	1.71(60)	E2	5181.3	18^+	→	16^+
996.7	2.0(0.3)	2.0	0.93(19)	1.70(55)	E2	5915.3	20^+	→	18^+
1045.9	10.9(2.2)	11.0	0.94(17)	1.49(40)	E2	4443.9	15^-	→	13^-

[a] determination of intensity and DCO ratio not possible due to x–rays
[b] line too weak for determination of DCO ratio
[c] multipolarity ambiguous, correction for internal conversion not possible

the coincidence relations between these transitions, their relative intensities and excitation energy sums and differences. Spin assignments were made on the basis of DCO ratios as described above. The strongly populated levels are grouped into several bands. They are the ground band and an excited positive–parity band, labeled AB in Fig. 2, and two negative–parity sequences, labeled AE/ABCE and AF, respectively.

The $8^+ \rightarrow 6^+$ transition of the ground band, which was only tentatively assigned in previous work [14], could be firmly established as a stretched quadrupole transition. Though a $10^+ \rightarrow 8^+$ transition is not observed, the existence of the 10^+ state is evident because of the 977.1 keV dipole transition which is feeding the 9^- state and because of the 94.2 keV transition depopulating the 12^+ state. Although the intensity of the 94.2 keV transition is too weak for a DCO analysis, the intensity flow taking into account internal conversion is consistent with E2 multipolarity. The AB band, which was previously known only up to the 14^+ state, is extended up to $I^\pi = 20^+$. Of the two bands with negative parity, the one which is built on the 5^- state (AE) is more strongly populated. It is crossed by another band at spin 17 (ABCE) which is observed up to spin 21^-. The second negative–parity band (AF) is built on the 6^- state and observed up to 14^-.

Besides those bands we establish many non–yrast levels which are connected by weak transitions. Although the DCO data are ambiguous in some cases of very weak transitions, the placement and spin assignment of those lines results in a consistent level scheme.

4 Discussion

The band structures observed in ^{200}Hg are very similar to those in the lighter Hg isotopes with even mass numbers [15]. However, there are some significant differences which shall be discussed here. The systematics of the excitation energy of the yrast positive– and negative–parity states in $^{190-200}$Hg is given in Fig. 3. The lighter isotopes are not considered here because of the occurrence of shape coexistence. The ground bands remain regular only up to the 6^+ state. A $\nu i_{13/2}$ two–quasineutron band intersects the ground band around spin 10 creating a triplet of close–lying states with spins 8^+, 10^+ and 12^+. According to the convention of the CSM [16] this two–quasineutron band is denoted AB.

The triplet of close–lying states has been investigated extensively in previous work including γ–ray, conversion–electron [17,18], lifetime [14,17,19,20] and g–factor measurements [21–23]. The results are consistent with the band–crossing picture with very small interaction energies between the ground and AB bands. The small interaction explains the reduced E2 transition probabilities in the band-crossing region.

In ^{198}Hg the transition probability B(E2) for the $8^+ \rightarrow 6^+$ transition is reduced by a factor of three compared to a collective transition [14] indicating that the interaction of the two crossing bands is weak. A second, higher–energy transition $8_2^+ \rightarrow 6^+$ has been observed with almost the full collective strength. Therefore, the second 8_2^+ state has been interpreted as the member of the ground band.

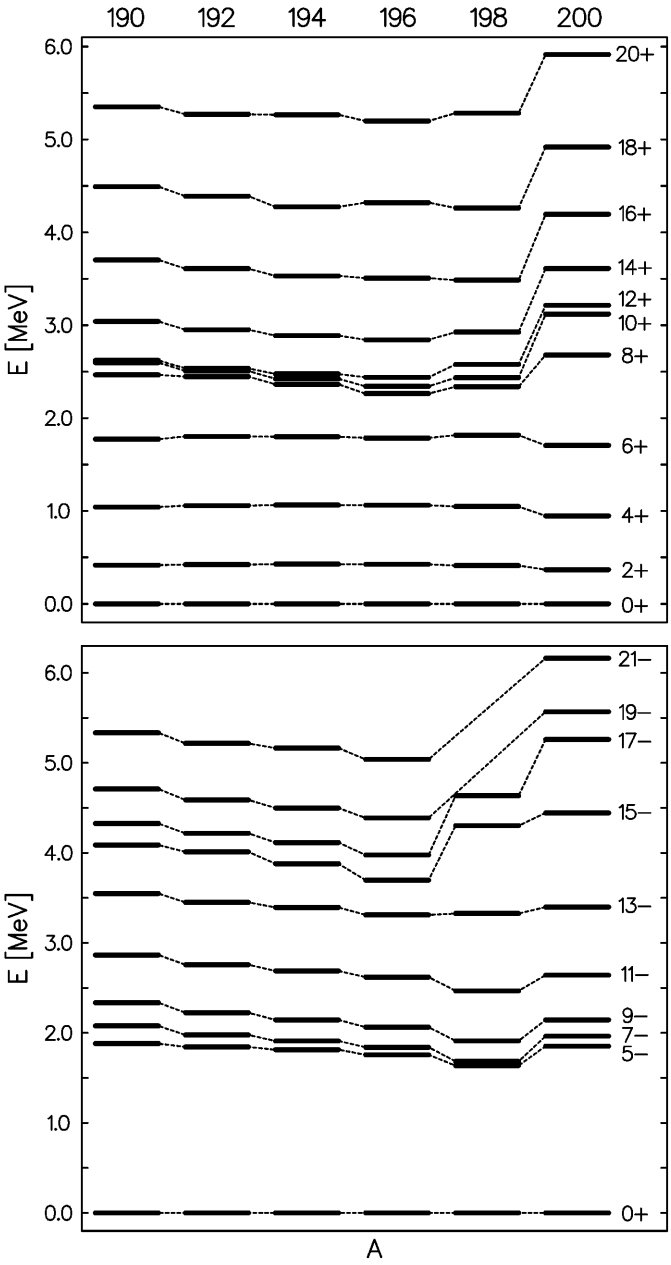

Fig. 3. Systematics of the excitation energy in the even Hg isotopes of the positive–parity yrast states (upper panel) and of the negative–parity states of the AE and ABCE bands, respectively (lower panel). Data are taken from [15] and present work

In ^{200}Hg the excitation energy of the 8^+ state lies much higher than in the lighter isotopes. Its energy and B(E2) value [14] are in perfect agreement with an interpretation as the ground band member. No transition is observed between the 10^+ and 8^+ states (see Fig. 2) which can be explained in the following way. For $N = 120$ the $\nu i_{13/2}$ subshell is filled and a large gap appears in the Nilsson energy–level scheme. Therefore, more energy is needed to

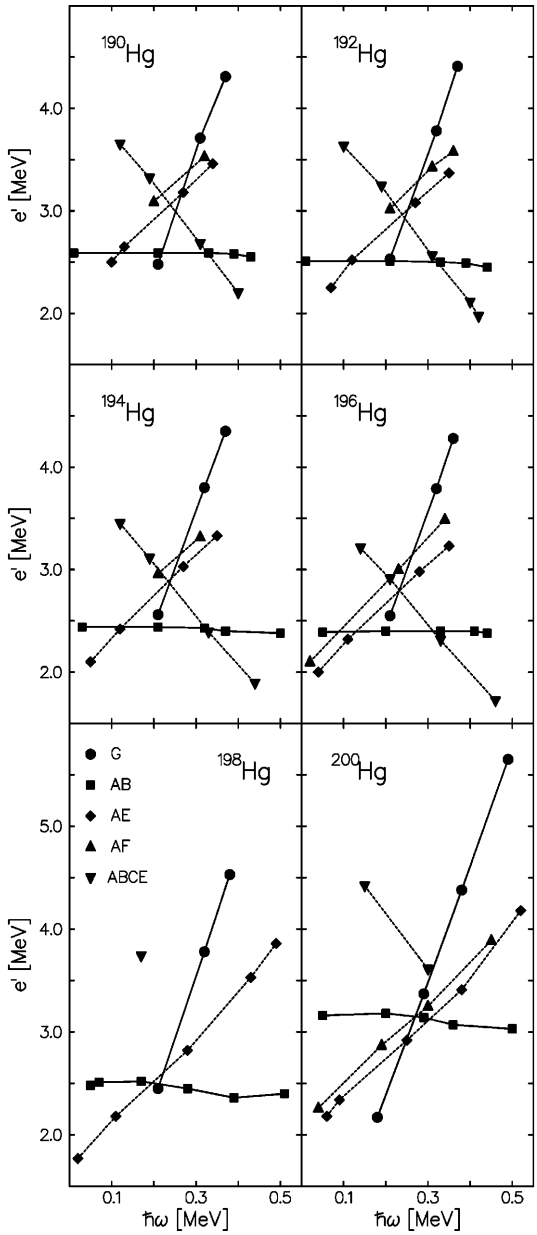

Fig. 4. Experimental Routhians for the isotopes $^{190-200}$Hg with even mass numbers. The AB band was taken as a reference with parameters $\mathcal{J}_0 = 8.0\hbar^2/MeV$, $\mathcal{J}_1 = 40\hbar^4/MeV^3$ and $i_{AB}^{ref} = 11.5\hbar$

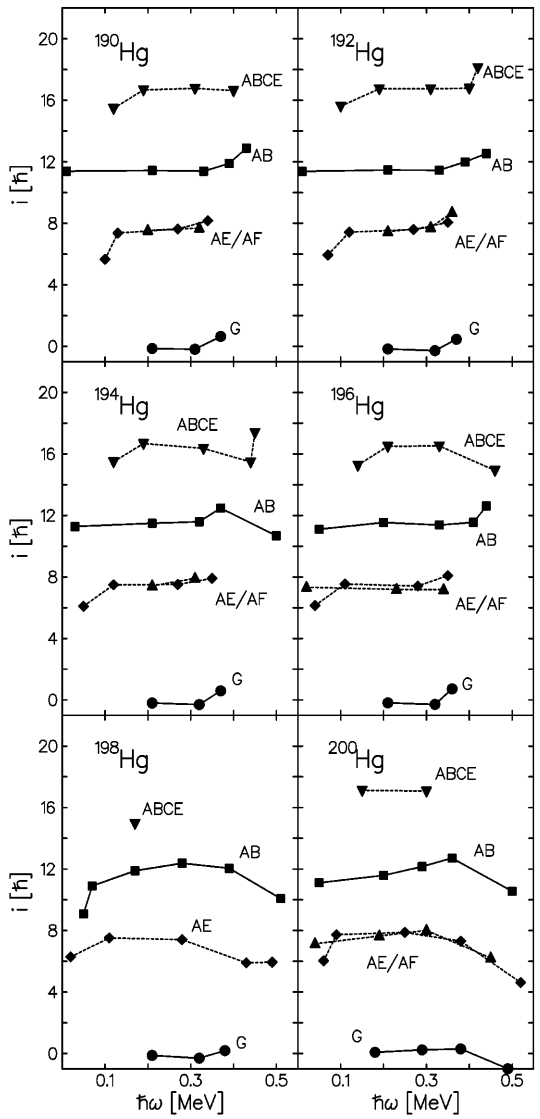

Fig. 5. Experimental alignments for the isotopes $^{190-200}$Hg with even mass numbers

excite an $i_{13/2}$ neutron pair. The higher excitation energy of the AB band of ^{200}Hg can be clearly seen in Fig. 3. As a consequence, the interaction between the AB and the ground band is smaller than in the lighter isotopes and the $10^+ \rightarrow 8^+$ E2 transition is strongly hindered. Instead, the AB band decays into the negative–parity bands AE and AF. This decay path is favoured because it involves E1 transitions and the rearrangement of only one $i_{13/2}$ quasineutron.

Also the negative–parity bands in ^{200}Hg are higher in excitation energy compared to the lighter Hg isotopes due to the closure of the $i_{13/2}$ subshell. For the AE band this can be clearly seen in the lower panel of Fig. 3. One of the negative–parity bands, the AE band, is crossed by a new structure, ABCE, with an additional rotation–aligned $i_{13/2}$ neutron pair at spin 17. The effect of the shell closure for the ABCE band is already observed in ^{198}Hg, as expected. In ^{200}Hg the alignment of the additional neutron pair results again in a higher excitation energy compared to ^{198}Hg. As for the ground and the AB band, also in this case the mixing between the AE and ABCE bands may be assumed to be smaller than in the lighter Hg isotopes. This would explain the rather large branching ratio of the 719 and 816 keV transitions.

Figures 4 and 5 compare the experimental Routhians and aligned angular momenta, respectively, for the even Hg isotopes. The two–quasineutron (AB) band is used in all cases as a common reference core with parameters $\mathcal{J}_0 = 8.0\hbar^2/MeV$, $\mathcal{J}_1 = 40\hbar^4/MeV^3$ and $i_{AB}^{ref} = 11.5\hbar$. The chain of isotopes shows a remarkably systematic be-

haviour. The Routhians are almost identical for ^{190}Hg to ^{198}Hg, only in ^{200}Hg the Routhians involving $i_{13/2}$ neutrons lie about 600 keV higher in energy due to the filled subshell, as discussed above. Consequently, the band crossing frequencies are also higher in ^{200}Hg than in the lighter isotopes: ω_{AB} increases from 0.21 to 0.27 MeV/$\hbar$ and ω_{BC} from 0.24 to 0.31 MeV/$\hbar$. As expected, the aligned angular momenta of 7.0, 11.6 and 17.1 $\hbar$ for the AE/AF, AB and ABCE bands, respectively, are in agreement with the ones observed in the lighter isotopes and with calculations within the framework of the CSM [1,2].

5 Summary

In summary, high–spin states in ^{200}Hg have been populated in the incomplete fusion reaction ^{198}Pt(^{9}Be,α3n) and γ–ray coincidences have been measured using the 8π spectrometer. The level scheme has been extended to higher spins and excitation energies. New band crossings are found and the band structures are compared to the ones in the lighter Hg isotopes with even mass numbers.

This work was supported by BMBF, Germany, and DoE, USA. A.G. acknowledges support from DAAD. The authors would like to thank the staff of the 88-Inch Cyclotron of the LBNL for excellent collaboration and David Radford for providing the RADWARE analysis package.

References

1. M. Guttormsen and H. Hübel, Nucl. Phys. A **380**, 502 (1982)
2. H. Hübel, A.P. Byrne, S. Ogaza, A.E. Stuchbery, G.D. Dracoulis, and M. Guttormsen, Nucl. Phys. A **453**, 316 (1986)
3. H. Helppi, S.K. Saha, M. Piiparinen, C.L. Dors, P.J. Daly, and T.L. Khoo, Phys. Rev. C **23**, 2345 (1981)
4. J. Wilczyński, K. Siwek–Wilczyńska, J. van Driel, S. Gonggrijp, D.C.J.M. Hageman, R.V.F. Janssens, J. Łukasiak, R.H. Siemssen, and S.Y. van der Werf, Nucl. Phys. A **373**, 109 (1982)
5. A. Gavron, Phys. Rev. C **21**, 230 (1980)
6. G.D. Dracoulis, A.P. Byrne, T. Kibédi, T.R. McGoram, and S.M. Mullins, J. Phys. G **23**, 1191 (1997)
7. T. Inamura, M. Ishihara, T. Fukuda, T. Shimoda, and H. Hiruta, Phys. Lett. **68B**, 51 (1977)
8. B.Bindu Kumar, S.Mukherjee, S. Chakrabarty, B.S. Tomar, A. Goswami, and S.B. Manohar, Phys. Rev. C **57**, 743 (1998)
9. M. Dasgupta, D.J. Hinde, R.D. Butt, R.M. Anjos, A.C. Berriman, N. Carlin, P.R.S. Gomes, C.R. Morton, J.O. Newton, A. Szanto de Toledo, and K. Hagino, Phys. Rev. Lett. **82**, 1395 (1999)
10. T. Udagawa and T. Tamura, Phys. Rev. Lett. **45**, 1311 (1980)
11. J.P. Bondorf, J.N. De, G. Fái, A.O.T. Karvinen, B. Jakobsson, and J. Randrup, Nucl. Phys. A **333**, 285 (1980)
12. F.S. Stephens, M.A. Deleplanque, R.M. Diamond, A.O. Macchiavelli, and J.E. Draper, Phys. Rev. Lett. **54**, 2584 (1985)
13. A. Galindo–Uribarri, D. Ward, H.R. Andrews, G.C. Ball, D.C. Radford, V.P. Janzen, S.M. Mullins, J.C. Waddington, A.V. Afanasjev, and I. Ragnarsson, Phys. Rev. C **54**, 1057 (1996)
14. C. Günther, H. Hübel, A. Kleinrahm, R. Kulessa, H. Emling, P. Fuchs, E. Grosse, D. Schwalm, H.J. Wollersheim, J. Idzko, and H. Ower, Z. Phys. A **301**, 119 (1981)
15. R.B. Firestone, V.S. Shirley, C.M. Baglin, S.Y.F. Chu, and J. Zipkin, eds., *Table of Isotopes* (J. Wiley and Sons, 1996)
16. R. Bengtsson and S. Frauendorf, Nucl. Phys. A **327**, 139 (1979)
17. R. Kroth, K. Hardt, M. Guttormsen, G. Mikus, J. Recht, W. Vilter, H. Hübel, and C. Günther, Phys. Lett. **99B**, 209 (1981)
18. M. Guttormsen, A. von Grumbkow, Y.K. Agarwal, K.P. Blume, K. Hardt, H. Hübel, J. Recht, P. Schüler, H. Kluge, K.H. Maier, A. Maj, and N. Roy, Nucl. Phys. A **398**, 119 (1983)
19. K. Hardt, Y.K. Agarwal, C. Günther, M. Guttormsen, R. Kroth, J. Recht, F.A. Beck, T. Byrski, J.C. Merdinger, A. Nourredine, D.C. Radford, J.P. Vivien, and C. Bourgeois, Z. Phys. A **312**, 251 (1983)
20. V. Kölschbach, P. Schüler, K. Hardt, D. Rosendaal, C. Günther, K. Euler, R. Tölle, M. Marten–Tölle, and P. Zeyen, Nucl. Phys. A **439**, 189 (1985)
21. R. Kroth, S.K. Bhattacherjee, C. Günther, M. Guttormsen, K. Hardt, H. Hübel, and A. Kleinrahm, Phys. Lett. **97B**, 197 (1980)
22. H. Sergolle, P. Aguer, G. Bastin, R. Kroth, J.P. Thibaud, K. Hardt, T. Lönnroth, F. Beck, and J.C. Merdinger, Z. Phys. A **313**, 289 (1983)
23. S.A. Hjorth, I.Y. Lee, J.R. Beene, C. Roulet, D.R. Haenni, N.R. Johnson, F.E. Obenshain, and G.R. Young, Phys. Rev. Lett. **45**, 878 (1980)